ChemElectroChem

Research Article
doi.org/10.1002/celc.202300834

Chemistry Europe
European Chemical Societies Publishing

www.chemelectrochem.org

Thin Coatings of Polymer of Intrinsic Microporosity (PIM-1) Enhance Nickel Electrodeposition and Nickel-Catalyzed Hydrogen Evolution

Jacopo Isopi,[a, b] Neil B. McKeown,[c] Mariolino Carta,[d] Giulia Tuci,[e] Giuliano Giambastiani,[f] Massimo Marcaccio,*[b] and Frank Marken*[a]

Nickel nanoparticle electrodeposition is studied on flat glassy carbon (GC) or on nitrogen-doped reduced graphene oxide (rGO-N) substrates. The effects of a very thin (nominally 16 nm) layer polymer of intrinsic microporosity (PIM-1) are investigated (i) on enhancing nickel nanoparticle nucleation and growth during electrodeposition and (ii) on enhancing hydrogen evolution electrocatalysis. Beneficial effects are tentatively assigned to PIM-1 suppressing blocking effects from interfacial hydrogen bubble formation. Exploratory data suggest that in aqueous 0.5 M NaCl solution (artificial seawater) nickel nanoparticles grown into a thin film of PIM-1 could be a viable electrocatalyst with an onset of hydrogen evolution only slightly negative compared to that observed for platinum nanoparticles.

1. Introduction

New technologies are required for the development of renewable and clean energy carriers, especially hydrogen (H_2), as a substitute for traditional fossil fuels.[1] Photocatalytic and/or electrocatalytic hydrogen evolution reactions (HER) will play an important part.[2] Although precious metals (Pt, Pd, Rh, *etc.*) are highly efficient HER catalysts, their higher cost and scarcity hinder their practical/sustainable application.[3] Hence, it is important to develop alternative catalysts with good efficiency, low cost and earth abundance. Recently, non-noble transition metals and their related compounds, including oxides, nitrides, phosphides, carbides and sulphides, have been investigated and demonstrated to potentially provide alternative catalysts for HER depending on the applied reaction conditions.[4,5] Particularly attractive for hydrogen evolution electrocatalysis were nickel/nickel sulfide,[6] molybdenum sulfide,[7] nickel phosphide,[8] and vanadium diselenide.[9]

In addition to exploring new catalytic materials, it is also possible to explore novel catalytic environments and confined catalysts. For example, supports or coatings of microporous materials on electrocatalysts could beneficially affect the catalytic reaction in terms of catalyst durability and kinetics. The surface of a hydrogen evolution catalyst causes "triphasic" conditions[10,11] in which gas|liquid|solid phase systems coexist and interact. The formation of gas bubbles close to or on the electrocatalytic interface can be an important factor affecting catalyst blocking or performance. Materials such as Polymers of Intrinsic Microporosity (PIMs) have been proposed to beneficially affect triphasic interfacial reactions by suppressing bubble nucleation and adhesion directly to catalyst surfaces.[12] The electrogenerated product can permeate through nano-channels in the PIM to then nucleate outside of the polymer film without blocking access to the catalyst surface. It is shown here, in a preliminary investigation, that this effect could be beneficial not only during the hydrogen evolution reaction with a nano-nickel catalyst, but also during the catalyst nanoparticle nucleation and electrodeposition process.

PIMs have been introduced into electrochemistry and catalysis over the last ten years[13,14,15] and have shown to provide highly molecular structure-dependent effects. PIMs have a highly rigid and contorted molecular backbone that creates poor packing/weak interactions in the solid/glassy state leaving accessible free volume. PIMs are electrical insulators. In electrochemical systems they can stabilise interfaces and change interactions for example with gas bubbles. Furthermore, PIMs are readily soluble into common solvents such as chloro-

[a] J. Isopi, F. Marken
Department of Chemistry, University of Bath, Claverton Down, Bath BA2 7AY, UK
E-mail: f.marken@bath.ac.uk

[b] J. Isopi, M. Marcaccio
Università di Bologna, Dipartimento Chimica "Giacomo Ciamician", Via Selmi 2, I-40126 Bologna, Italy
E-mail: massimo.marcaccio@unibo.it

[c] N. B. McKeown
EaStCHEM, School of Chemistry, University of Edinburgh, Joseph Black Building, David Brewster Road, Edinburgh, Scotland EH9 3JF, UK

[d] M. Carta
Department of Chemistry, Faculty of Science and Engineering, Swansea University, Grove Building, Singleton Park, Swansea SA2 8PP, UK

[e] G. Tuci
Institute of Chemistry of Organometallic Compounds, ICCOM-CNR and INSTM Consortium, Via Madonna del Piano 10, 50019 Sesto Fiorentino (Florence), Italy

[f] G. Giambastiani
Università di Firenze, Dipartimento Chimica "U. Schiff", Via della Lastruccia 3–13, I-50019 Sesto F.no (Firenze), Italy

Supporting information for this article is available on the WWW under https://doi.org/10.1002/celc.202300834

form and THF. They are readily cast into highly microporous film structures with typically 1 nm diameter pores and channels.[16] PIMs with tertiary amines in the backbone are known to show pH dependent protonation and anionic conductivity.[17] They have been employed in ionic current rectifying nano-membranes[18] and used to immobilise catalysts at electrode surfaces.[19] PIMs with more hydrophobic channels have been employed in photoelectrochemistry,[20] as a precursor for porous carbon,[21] in lithium-ion batteries,[22] and in membranes for redox flow systems.[23–25] In this study, the microporous polymer PIM-1 (Scheme 1) is employed, which has been investigated previously, for example, for the absorption[26] and permeation/separation of gases.[27]

In this work, the electrodeposition of nickel nanoparticles as non-noble metal electrocatalyst is investigated. Nickel and nickel alloys are known to have good catalytic properties for many applications[28,29] and are appropriate for hydrogen evolution in aqueous 0.5 M NaCl. Nickel nanoparticles are formed on either glassy carbon (GC) or on N-doped reduced graphene oxide (rGO-N). This nickel electrocatalyst is then investigated in the absence or in the presence of a PIM-1 coating (Scheme 1). Preliminary experiments are performed by first electrodepositing nano-nickel followed by PIM-1 coating or by directly electrodepositing nano-nickel into the microporous PIM-1 film on a carbon substrate. Preliminary data suggest that the latter approach proves to be more effective for producing better nickel nanoparticle plating results and more effective for making an active hydrogen evolution electrocatalyst as long as the PIM-1 film is very thin.

2. Results and Discussion

2.1. Electrolytic Formation of Platinum and Nickel Nanoparticle Catalysts

Nanoparticle deposits were produced by cycling the applied potential. Prior to each nanoparticle growth experiment, the support was carefully cleaned by polishing (see experimental section). Figure 1A shows data for the electrodeposition of Ni nanoparticles (Ni-NPs) on glassy carbon. The nickel deposition (standard potential $E^o(Ni^{2+}/Ni) = -0.56$ V vs. SHE) is accompanied by hydrogen evolution, and both processes are monitored simultaneously as a process starting at $E = -0.56$ V vs. SHE. It can be inferred that the higher is the population of nanoparticles on the electrode surface (with time/cycles), then the higher is the electrode hydrogen evolution activity; the current peak at −0.89 V vs. SHE corresponds to the hydrogen evolution signal in this solution. In a similar manner, platinum nanoparticles (Pt-NPs) were successfully grown onto either glassy carbon (Pt-GC) or on N-doped reduced graphene oxide (Pt-rGO-N). Figure 1B shows a typical set of cyclic voltammetry data during Pt-NP growth on bare glassy carbon (standard potential $E^o(PtCl_6^{2-}/Pt) = 0.74$ V vs. SHE). The magnitude and shape of the voltammetric signal suggest hydrogen evolution on the freshly grown platinum catalyst. By cycling the applied potential, the catalyst activity can be monitored. In addition, a small hydrogen oxidation signal is observed when reversing the scan direction to more positive potentials. From a comparison of data sets in Figure 1, it is evident that both sets of voltammograms are dominated by the hydrogen evolution. This explains the current increase that starts at −0.2 V vs. SHE on Pt-GC and at more negative potential (−0.7 V vs. SHE) on Ni-GC.

Figure 2 shows SEM images for Ni-NPs grown on glassy carbon (A–B), Ni-NPs grown on rGO-N (C–D) and Pt-NPs grown on glassy carbon (E–F). As an electrodeposition procedure, 18 potential cycles were employed under conditions as shown in Figure 1. While Ni-NPs on GC have an average diameter of typically about 80 nm, those grown on rGO<-N have a mean diameter of typically about 35 nm (see Figure 2).

Figure 3 shows typical hydrogen evolution reaction (HER) voltammograms for Ni-GC and Ni-rGO-N immersed in a 0.5 M NaCl aqueous solution. The solution is unbuffered (representing conditions similar to those in seawater) and therefore hydrogen evolution is accompanied by hydroxide formation, thus causing a drift in pH value locally at the electrode surface. As a result,

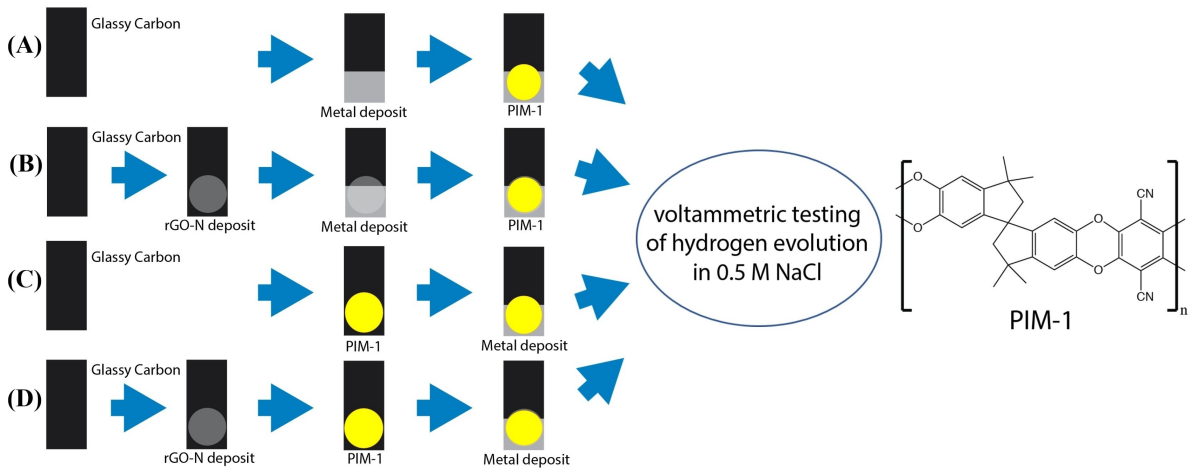

Scheme 1. Schematic drawing of four routes (**A**–**D**) to electrodeposition of nickel nanoparticles catalyst on a carbon surface (either glassy carbon or reduced N-doped graphene oxide) and embedded into a PIM-1 coating (applied either before or after metal deposition).

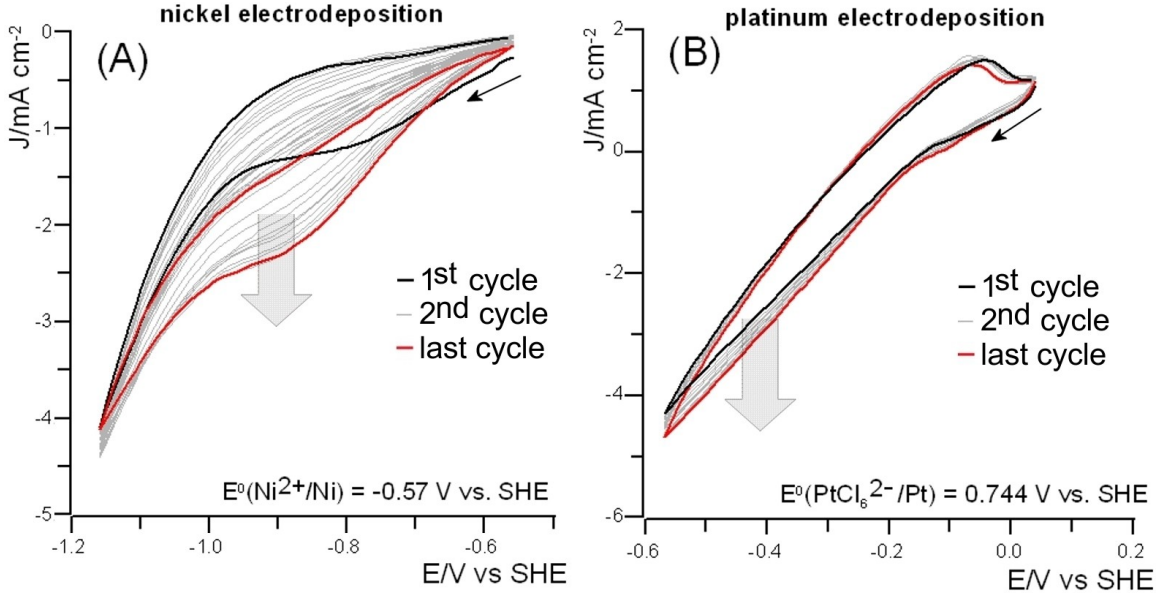

Figure 1. Cyclic voltammetry data (scan rate 50 mV s^{-1}, T = 22 °C) for metal nanoparticles growth. Electrode surface progressive modification followed by current magnitude changes over subsequent potential cycles. (A) Nano-nickel growth in 70 mM KCl, 30 mM L-ascorbic acid, 1 mM $NiCl_2$ on bare GC. (B) Nano-platinum growth in 70 mM KCl, 30 mM L-ascorbic acid, 1 mM K_2PtCl_6 on bare GC.

voltammograms are broadened and shifted to more negative potentials. Moreover, such an increase of local pH during the Ni^{2+} ion reduction to form NPs leads to generate an oxide layer on the Ni NPs themselves.[30] The bare glassy carbon electrode exhibits hydrogen evolution activity at more negative potentials (Figure 3A). In the presence of Ni, hydrogen evolution starts at −0.61 V vs. SHE for Ni-GC and at −0.46 V vs. SHE for Ni-rGO-N. Figure 3B shows data for platinum nanoparticles indicative of a reversible potential for hydrogen evolution under these conditions close to −0.61 V vs. SHE. The hydrogen evolution is shifted negative from the expected value at −0.41 V vs. SHE for pH 7 due to unbuffered conditions and local formation of hydroxide at the working electrode surface.

2.2. The Effect of PIM-1 on Hydrogen Evolution

Next, a volume of 2 μL of PIM-1 (1 mg/mL in chloroform) was drop-cast on Ni-GC and Ni-rGO-N electrocatalysts (Scheme 2B). The coated area is approximately 5 mm×5 mm to give an average film thickness of 80 nm (assuming a polymer density of approx. 1 g cm^{-3}).[31] The PIM-1 coating led to a net increase of HER activity, as shown in Figures 3B. In addition, Figure 3C clearly shows the presence of a "noisy" current in the absence of PIM-1 coating on Ni-rGO-N. This behaviour can be explained as the consequence of interfacial generation of hydrogen bubbles that interfere with the catalytic process and hence apparently reduces the catalyst efficiency by partially blocking access to the surface. It appears that the PIM-1 coating can prevent bubble adhesion to the surface and blocking of the electrode or catalyst. Ni-NPs remain in contact with the aqueous solution phase (*via* microporous PIM-1) and HER activity is maintained. The polymer may also beneficially affect adhesion of the Ni-NPs to the substrate. This result prompted us to evaluate the opportunity to grow Ni-NPs directly into PIM-1 coated electrodes (see Scheme 2C).

2.3. The Effect of PIM-1 on Electrolytic Nanoparticle Synthesis

Next, the effects of PIM-1 on the nickel electro-deposition were investigated. PIM-1 was first drop-cast onto GC or onto rGO-N producing a thicker PIM-1 deposit in the centre and a thinner PIM-1 film at the edges. Subsequently, the metal electro-deposition was carried out (Scheme 2C) generating an uneven nanoparticle film depending on the PIM-1 film thickness. SEM images (Figure 4) show a preferential area for nanoparticle growth located in the thinner film regions, hence close to the PIM-1 edges. Indeed, only a few Ni-NPs were observed outside of the PIM-1 film region and almost none were detected in the central thicker PIM-1 coated area. This evidence suggests that only a very thin deposit of PIM-1 facilitates nickel nucleation/growth processes. Such a film may also help preventing H_2 bubbles from blocking or dislodging the growing nickel nanoparticles. In the case of PIM-1 coated rGO-N, Ni-NP electrosynthesis failed (Figure 4D) likely due to a less controlled overall thicker PIM-1 deposit obtained on the rougher rGO-N surface.

In additional experiments, a five-fold dilute solution of PIM-1 (0.2 mg/mL in chloroform) was prepared and drop-cast to ensure a thinner PIM-1 deposit on either GC and rGO-N coated GC. Under these dilute conditions (the average PIM-1 nominal thickness is only 16 nm) the formation of a much higher nickel particle density is observed along with a more homogeneous distribution under the thin PIM-1 coating on both GC or on rGO-N substrate. Figures 5A, B show SEM images for Ni-NPs grown into a PIM-1 coated GC electrode. Similarly, Figures 5C

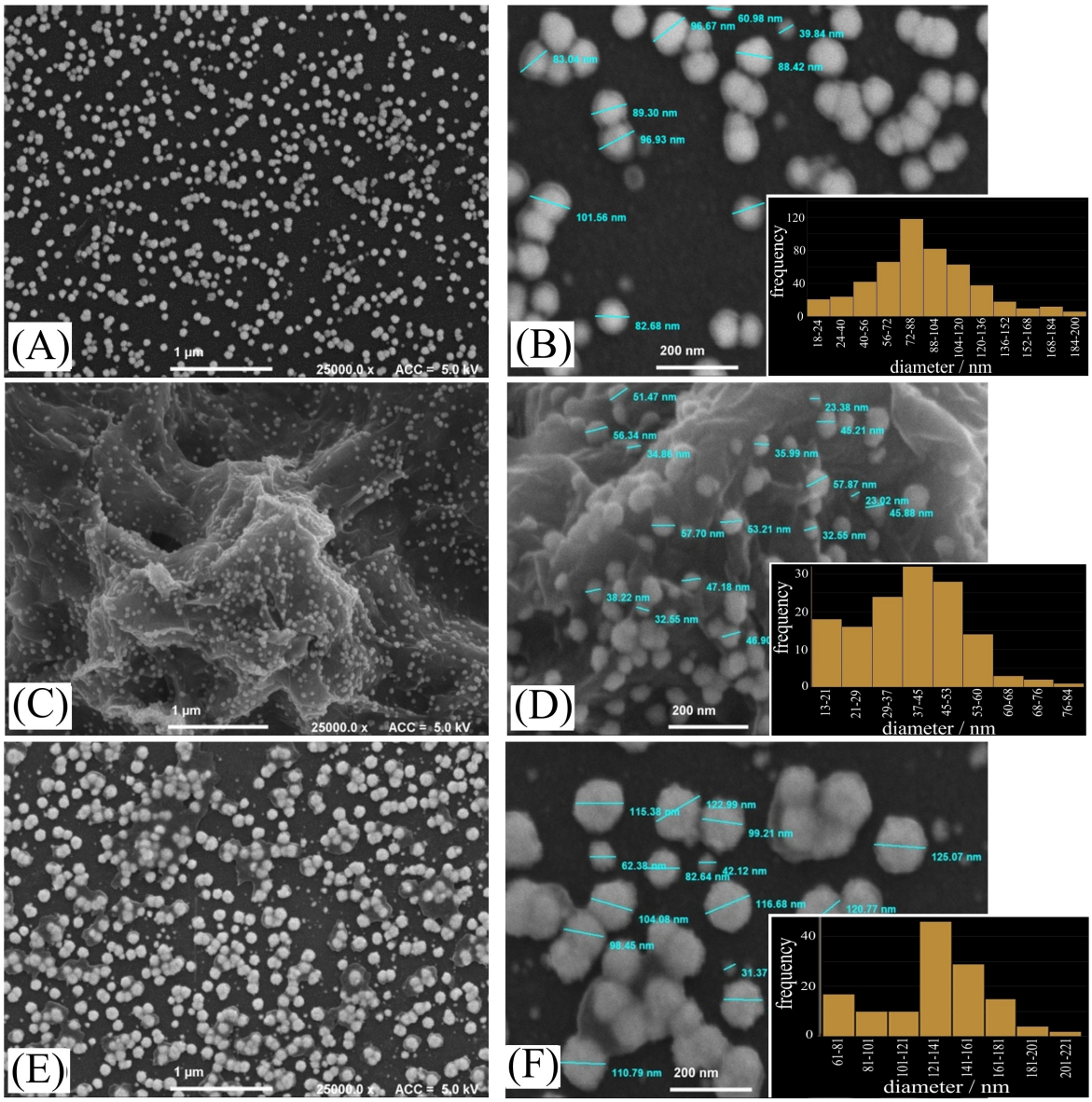

Figure 2. (A–B) SEM images of nickel nanoparticles grown on flat glassy carbon. Magnification 25 K (A), 100 K (B). (C–D) SEM images of Ni nanoparticles grown on rGO-N. Magnification 25 K (C), 100 K (D). (E–F) SEM images of Pt nanoparticles grown on GC. Magnification 25 K (E), 100 K (F). Histograms show particle size distributions statistics.

and 5D show Ni-NPs grown into a thin PIM-1 film deposited on the rGO-N coated GC electrode. Note that the Ni-NPs are relatively big compared to the PIM-1 film thickness and therefore it is not known whether Ni-NPs grow through the polymer film or still have a PIM-1 polymer coating. Perhaps interestingly, Figure 5A show an apparent radial distribution of the NPs that can be attributed to the PIM-1 film arrangement on the surface electrode by drop-casting.

Moreover, Ni-NP electrodeposition into a thin PIM-1 film gave voltammetric responses consistent with well-performing hydrogen evolution electrocatalysts. Preliminary voltammetric data for hydrogen evolution in 0.5 M NaCl are shown in Figure 6. For Ni-NPs electrodeposited into thin PIM-1 films (Figure 6A), Ni-NPs on glassy carbon outperformed electrodes prepared on rGO-N. For Ni-NPs prepared by electrodeposition into a thin PIM-1 film on glassy carbon, the comparison with bare electrodeposited Pt-NPs on GC (Figure 6B) shows competitive performance for the nickel electrocatalyst coated electrode with only a slightly more negative overpotential for hydrogen evolution. It is worth noting that as currents approach 9–10 mA cm^{-2} the performance of the two electrodes becomes comparable.

These preliminary data suggest that Ni-NPs grown into a thin PIM-1 film (nominally 16 nm) coated GC electrode could generate a competitive HER electrocatalyst potentially appealing for application such as seawater electrolysis, although much more work will be required to address catalyst durability under more realistic conditions. The formation of Ni-NPs during electrodeposition into a thin PIM-1 film appears more effective possibly due to (i) enhanced nucleation and/or (ii) less bubble-

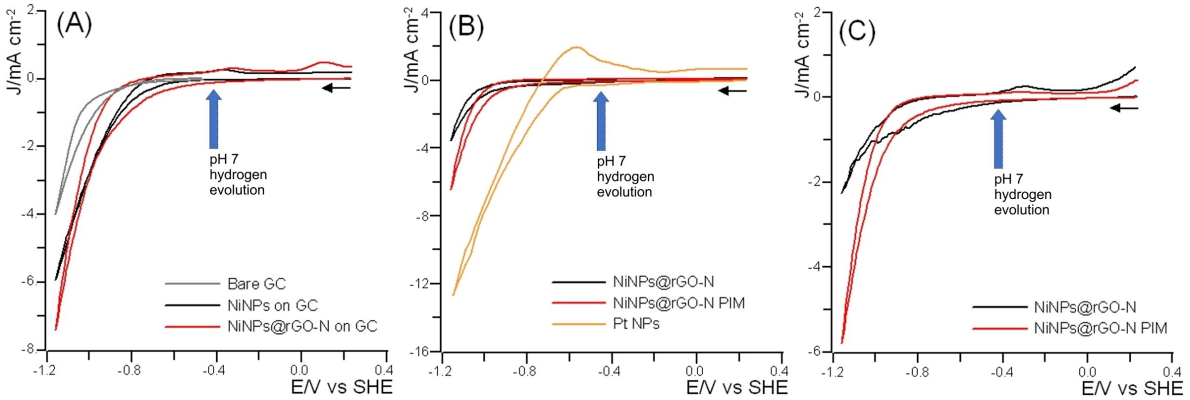

Figure 3. (A) Cyclic voltammetry data in 0.5 M NaCl aqueous solution (scan rate 50 mV s^{-1}, T = 22 °C) for two Ni-based electrocatalysts (Ni-GC and Ni-rGO-N). The background for bare glassy carbon is shown for comparison. (B) Cyclic voltammetry data (scan rate 50 mV s^{-1}) in 0.5 M NaCl with a comparison of catalytic hydrogen evolution for nickel nanoparticles on rGO-N without PIM-1 (black) and with PIM-1 (red). Data for platinum nanoparticles on GC (orange). (C) Data showing the effect of the PIM-1 film on nickel nanoparticles on rGO-N when hydrogen bubble formation occurs.

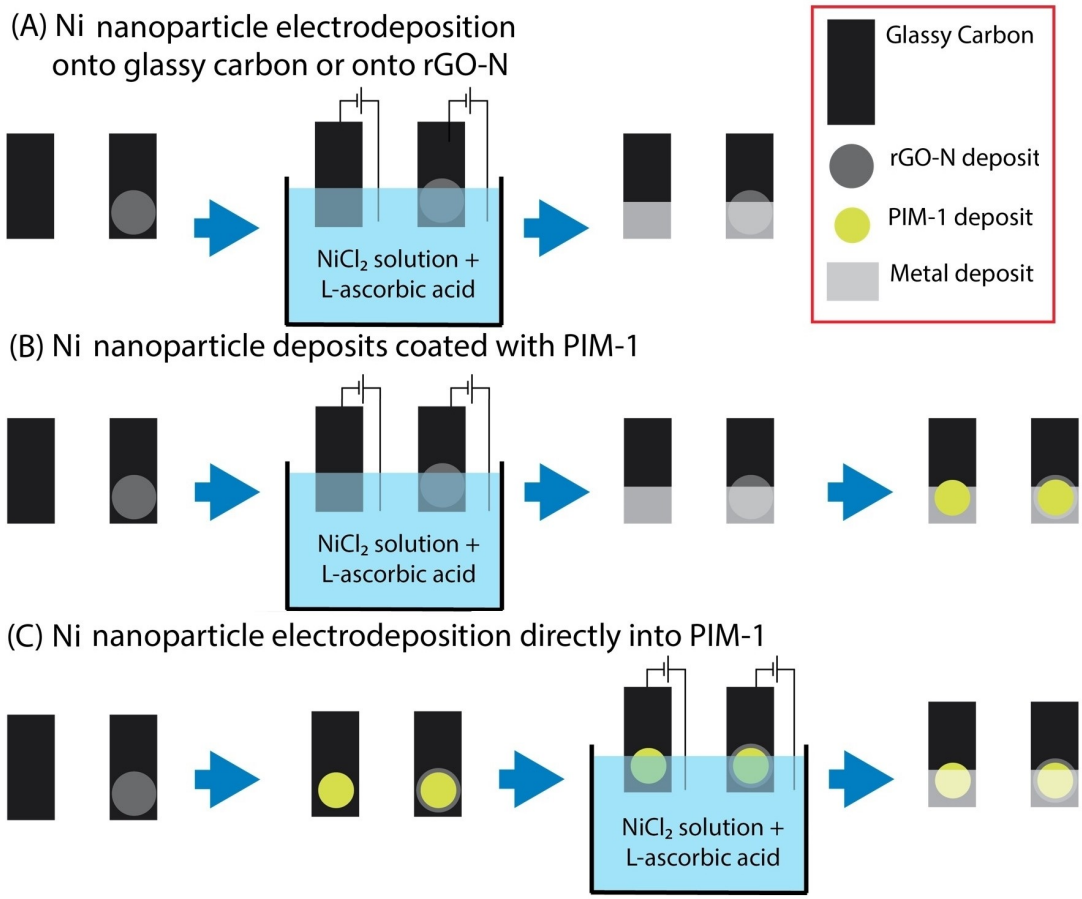

Scheme 2. (A) Schematic representation of the experimental procedure for Ni-NPs deposit on either flat glassy carbon (GC) or rGO-N coated glassy carbon. (B) The nickel-electrocatalysts are coated with a thin film of PIM-1. (C) The thin film of PIM-1 is applied before the electrodeposition of Ni-NPs.

induced removal of nickel nuclei from the electrode surface. Thin PIM-1 coatings could be effective also for other types of metal electrodeposition processes.

A combination of nickel nanoparticles with thin PIM-1 coating could be useful to improve NP adhesion to the support, thus potentially making the system more robust during hydrogen evolution. Concerning the stability of the Ni NPs/PIM-1 system, only short term tests have been performed (Figure S1 in the Supporting Information), as Pt counter electrodes should be avoided or used together with an ion-exchange membrane to prevent Pt re-deposition during the study of HER catalysis.[32] Problems due to Pt transfer and interference could arise in a

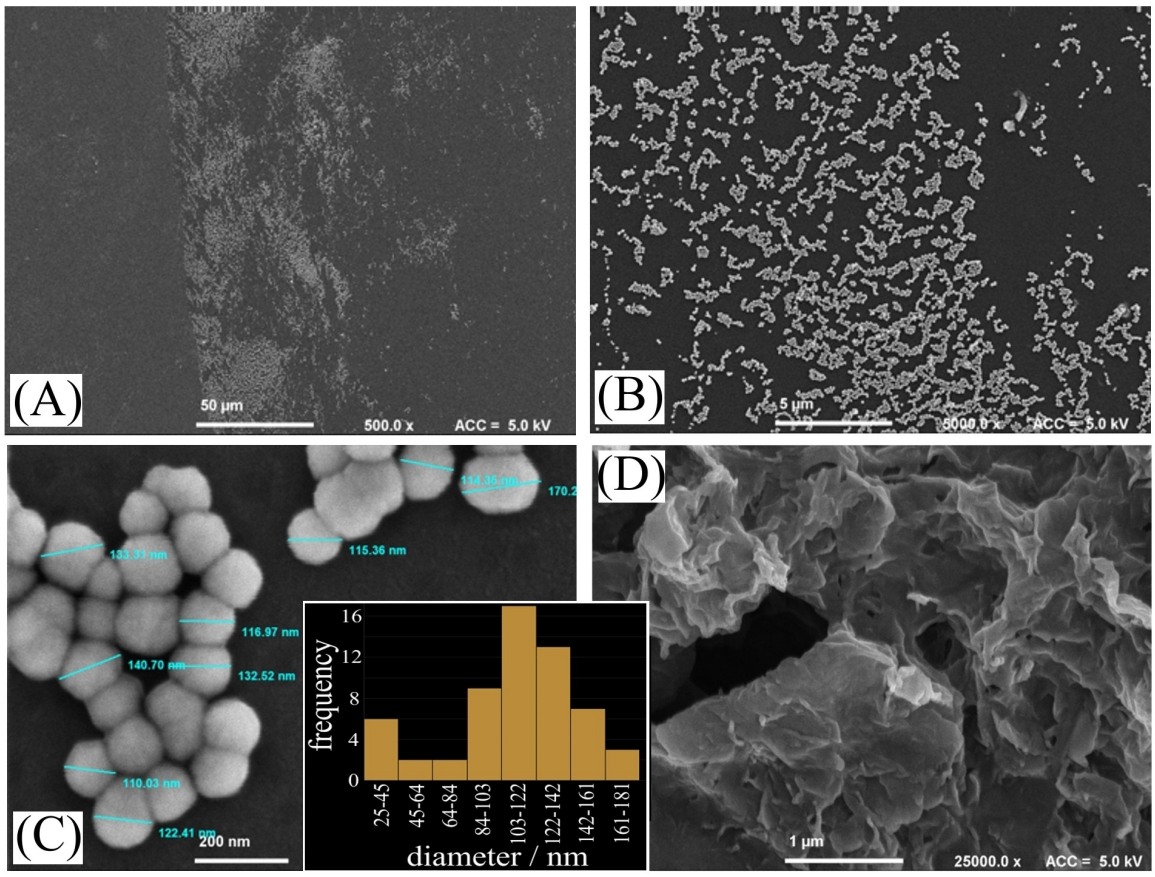

Figure 4. (A,B,C) SEM images of Ni nanoparticles grown under the PIM-1 film. The area with highest nanoparticle density is near the edge of the PIM-1 film in a thinner region. Magnification 500 (A), 5 K (B), 100 K (C). (D) No visible nanoparticles growth on rGO-N under PIM-1. Histogram shows particle size distribution statistics.

long term catalyst test. More work will be required on the durability and performance of these types of catalytic films (in view of reports on PIMs employed in fuel cell catalysis[33]) under more realistic conditions (higher currents, long term testing, higher areas, *etc.*). The adhesion/degradation of PIM-1 films under the harsh conditions of electrolytic hydrogen gas evolution will need to be studied more carefully on a wider range of substrates and over prolonged time. Finally, improved (molecularly designed) polymers of intrinsic microporosity materials could be developed in the future to provide not only triphasic gas permeation properties, but also good adhesion and long-term stable catalytic performance.

3. Conclusions

It has been shown that well-defined nickel nanoparticles electrodeposits (typically 100 nm diameter) can be formed by electrodeposition directly into a very thin coating of PIM-1 (nominally 16 nm thickness). The resulting hydrogen evolution catalyst was shown to be improved by the PIM-1 coating (probably due to suppression of interfacial gas bubble formation/adhesion and the resulting blocking of the catalyst). This type of electrode was shown to be at least qualitatively competitive (at higher current densities and for short durations) when compared to platinum NP-based hydrogen evolution electrocatalyst on the same substrate. The thickness of the PIM-1 film coating proved to be a critical parameter, as thicker deposits of PIM-1 suppressed nickel electrodeposition. A thin PIM-1 coating, however, enhanced nickel nanoparticle electrodeposition compared to the case of a bare glassy carbon electrode. Effects of thin PIM-1 films could be beneficial on processes in larger scale electrolyser systems and for higher current densities, but still need to be investigated. For larger scale, the chemical strategy for electrode production needs to be more sustainable.

Under these conditions, there was no further beneficial effect from employing r-GO-N and therefore simple glassy carbon support materials are sufficient. The effect of PIM-1 coatings on suppressing interfacial gas bubble nucleation/adhesion close to the electrode/catalyst surface could be beneficial (*e.g.* for mechanically stabilising the nanoparticle decorated interface) in other areas of electrochemical technology such as water splitting and fuel cell systems. Even just preventing bubble nucleation at the catalyst surface could be beneficial by avoiding mechanical stresses. A wider range of molecularly designed PIM materials could be synthesised and tested for specific catalytic gas evolution applications.

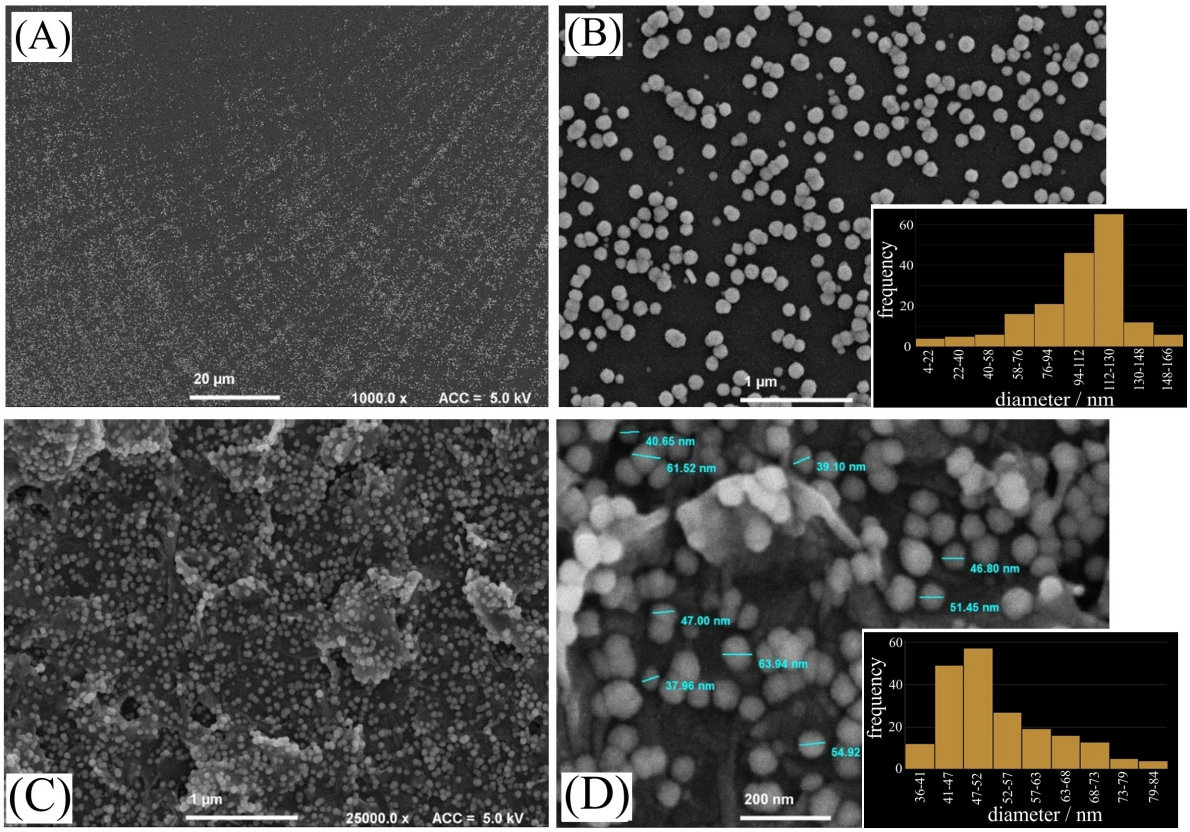

Figure 5. (A,B) SEM images for PIM-1 coated Ni-GC for electrolytic Ni growth into a thin PIM-1 film. By reducing the PIM film thickness NPs deposit uniformly. Magnification 1 K (A), 25 K (B). (C,D) SEM images for PIM-1 coated Ni-rGO-N for electrolytic Ni growth into a thin PIM-1 film. With a thinner film NPs electrodeposit successfully on rGO-N. Magnification 25 K (A), 100 K (B). Histograms show particle size distribution statistics.

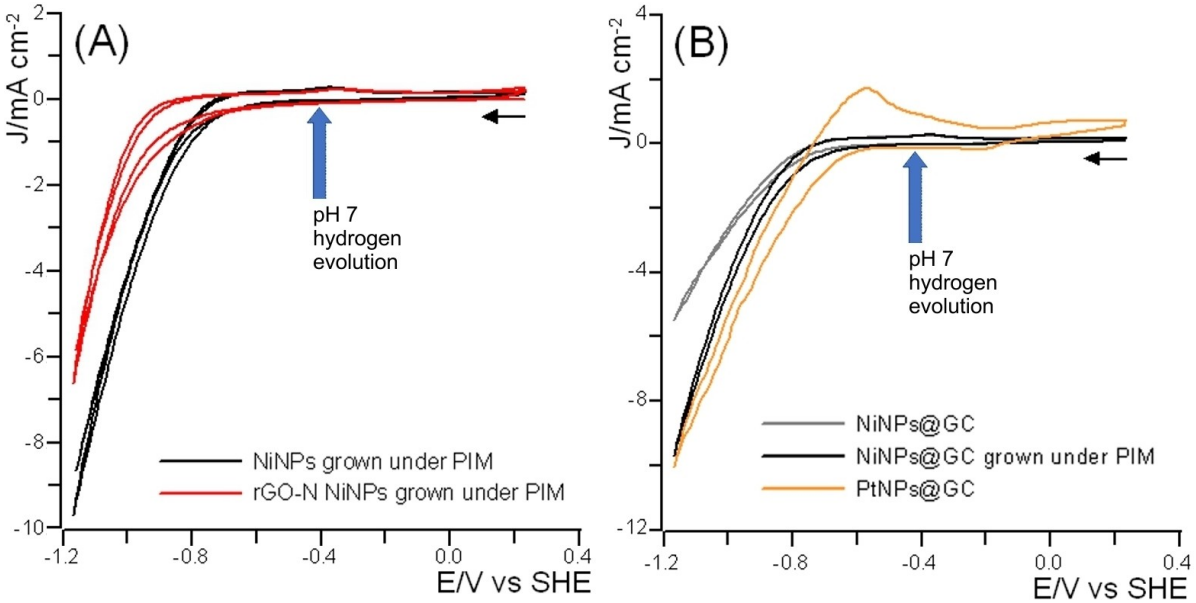

Figure 6. (A) Cyclic voltammetry data (two potential cycles, scan rate 50 mV s^{-1}, T = 22 °C) in 0.5 M NaCl showing the catalytic hydrogen evolution efficiency for Ni NPs grown into a PIM-1 film on GC or on rGO-N. (B) As before, but comparing Ni NPs on GC (grey), Ni NPs electrodeposited into PIM-1 on GC (black), and Pt NPs on GC (orange).

Experimental Section

Chemical Reagents. L-ascorbic acid ($C_6H_8O_6$, ≥ 99%), KCl (≥ 99%), $NiCl_2$ (98%), K_2PtCl_6 (98%), $N_2H_4 \cdot H_2O$ (98%), chloroform (≥ 99.5%), acetone (99.5%), isopropyl alcohol (≥ 98%), dichloromethane (≥ 99.8%), dimethylformamide (DMF ≥ 99.9%), ethanol (96%), and NaCl (≥ 99.5%) were obtained from Sigma-Aldrich and used without further purification. PIM-1 was synthesised following a literature procedure reported elsewhere.[34] Argon (Pureshield, BOC) was employed to de-aerate electrolyte solutions. Aqueous solutions were prepared with ultra-pure water of resistivity not less than 18.2 MΩ cm (at 20 °C) from a Thermo Scientific water purification system.

Instrumentation. Electrochemical experiments were performed in a glass cell (custom-made), with a platinum wire as counter electrode (CE, used here as an inert counter electrode, at least under mild conditions, for short measurement times, and for low current densities[35]), a KCl-saturated calomel electrode (SCE) as reference electrode (RE), and with an Ivium Compactstat potentiostat (Ivium, Netherlands). The working electrode (WE) was prepared from glassy carbon (Tokaicarbon.com, fine carbon SA-1). Electrochemical characterization was carried out in a 0.5 M NaCl solution. All current data were scaled to give a current density assuming a 5 mm ×5 mm electrode area. Potential data were calibrated to the standard hydrogen electrode (SHE) by shifting data by −241 mV (assuming approx. 25 °C conditions[36]). Scanning Electron Microscopy (SEM) images were obtained using a field-emission scanning electron microscope (FESEM, JEOL JSM-6301F) after keeping samples in vacuum for 24 hours and with an applied 10 nm chromium coating. SEM images were processed and analyzed by using the software ImageJ (release 1.54 h) to obtain the NPs size distribution statistics.

Sample preparation procedures. Nickel nanoparticles (Ni-NPs) were formed by electrodeposition on a flat glassy carbon electrode (GC, Tokai Carbon). The electrode was approx. 10 mm ×5 mm cut with a diamond blade and reused after cleaning and polishing. Before every experiment the GC slab was polished manually with a cloth (Buehler microcloth) and 0.3 micron alumina (Buehler, UK). After rinsing with distilled water, the polished electrode was sonicated for 5 min in acetone and for 15 min in isopropanol. Finally, rinsing with dichloromethane completed the last washing step. The back side of the GC was insulated with Kapton polymer tape. Two chloroform solutions of the PIM-1 polymer were prepared with concentrations of 1 mg/mL and 0.2 mg/mL. A single 2 μL drop cast onto the surface was sufficient for the PIM-1 film formation over a 5 mm×5 mm surface.

For the preparation of rGO-N coated electrodes, an amount of 40 μg of rGO-N (from a DMF/EtOH 1/1 ratio 1 mg/mL suspension; 8 portions of 5 μL) was deposited on the GC electrode before the nanoparticle electrodeposition. N-doped reduced graphene oxide (rGO-N) was synthesized following a slightly modified literature procedure.[37,38] An amount of 40 mg of GO prepared with a modified Hummers' method[39] was suspended in 40 mL of distilled water and sonicated for 30 minutes. Next, $N_2H_4 \cdot H_2O$ (0.015 mL) was added dropwise and the suspension stirred at 80 °C for 20 hours. After cooling to room temperature, the mixture was filtered through a PTFE membrane filter (0.2 μm), the solid recovered, suspended in distilled water and purified by dialysis. Finally, the suspension was filtered again and dried to constant weight.

Nanoparticle electrodeposition. Nanoparticles (NPs) were deposited onto an electrode substrate via electrodeposition of either 1 mM $NiCl_2$ for Ni-NPs or 1 mM K_2PtCl_6 for Pt-NPs from a solution containing 70 mM KCl and 30 mM L-ascorbic acid. Ascorbic acid is employed here as a capping agent to give well-defined nanoparticle deposits. Deposition of nickel was accomplished by cyclic voltammetry in the potential range from −0.8 V to −1.4 V vs. SCE by a total of 18 potential cycles at a scan rate of 50 mVs^{-1}. Platinum was electrodeposited in the potential range from −0.2 V to −0.8 V vs. SCE. As shown in Scheme 2, Ni-NP electrodeposition was carried out on two different supports: a flat glassy carbon (GC) or a rougher N-doped, reduced graphene oxide (rGO-N) coated GC. In addition, a thin coating of PIM-1 was deposited over the electrode surfaces (Scheme 2B). Alternatively, the PIM-1 film was applied first before Ni-NP electrodeposition as a microporous host matrix for metal nanoparticles to grow into (Scheme 2C).

Acknowledgements

University of Bologna is gratefully acknowledged for financial support. J.I. acknowledges a "Marco Polo" visiting grant to finance the leave period for research at the University of Bath. This study was carried out within the NEST–Network for Energy Sustainable Transition and received funding from the European Union Next-Generation EU (PIANO NAZIONALE DI RIPRESA E RESILIENZA (PNRR)–MISSIONE 4 COMPONENTE 2, INVESTIMENTO 1.3), CUP: J33C22002890007. This research was funded by the European Union – Next-Generation EU from the Italian Ministry of Environment and Energy Security POR H2 AdP MMES/ENEA with involvement of CNR and RSE, PNRR – Mission 2, Component 2, Investment 3.5 "Ricerca e sviluppo sull'idrogeno", CUP: B93C22000630006. G. G. and G. T. would like to thank the Italian MUR through the PRIN2022 project "MATISSE - A "Molecular Lift" for the Control of the Metal Protrusion and Coordination Sphere in Single-Atom Catalysts for CO_2 Electroreduction (2022K5SX27). F.M. thanks EPSRC for support (EP/K004956/1).

Conflict of Interests

The authors declare no conflict of interest.

Data Availability Statement

The data that support the findings of this study are available from the corresponding author upon reasonable request.

Keywords: hydrogen energy · sustainability · metal nanoparticles · electrolysis · gas evolution

[1] J. D. Fonseca, M. Camargo, J. M. Commenge, L. Falk, I. D. Gil, *Int. J. Hydrogen Energy* **2019**, *44*, 9486–9504.
[2] A. A. Ismail, D. W. Bahnemann, *Sol. Energy Mater. Sol. Cells* **2014**, *128*, 85–101.
[3] C. Acar, I. Dincer, G. F. Naterer, *Int. J. Energy Res.* **2016**, *40*, 1449–1473.
[4] P. Yu, F. M. Wang, T. A. Shifa, X. Y. Zhan, X. D. Lou, F. Xia, J. He, *Nano Energy* **2019**, *58*, 244–276.
[5] J. M. Wei, M. Zhou, A. C. Long, Y. M. Xue, H. B. Liao, C. Wei, Z. C. J. Xu, *Nano-Micro Lett.* **2018**, *10*, 75.
[6] C. C. Miao, X. W. Zheng, J. M. Sun, H. Wang, J. Qiao, N. Han, S. P. Wang, W. Gao, X. H. Liu, Z.-X. Yang, *ACS Appl. Energ. Mater.* **2021**, *4*, 927.
[7] L. Z. Bian, W. Gao, J. M. Sun, M. M. Han, F. L. Li, Z. F. Gao, L. Shu, N. Han, Z.-X. Yang, A. M. Song, Y. Q. Qu, J. C. Ho, *ChemCatChem* **2018**, *10*,1571.

[8] C. C. Miao, Y. M. Zang, H. Wang, X. M. Zhuang, N. Han, Y. X. Yin, Y. D. Ma, M. Chen, Y. Dai, S. P. Yip, J. C. Ho, Z.-X. Yang, *Adv. Mater. Interfaces* **2022**, *9*, 2200739.
[9] C. C. Miao, T. Zhang, F. L. Li, L. Zhang, J. M. Sun, D. Liu, L. Q. Wu, H. Wang, F. H. Chen, L. B. He, *Nanotechnology* **2021**, *32*, 265402.
[10] E. Madrid, J. P. Lowe, K. J. Msayib, N. B. McKeown, Q. L. Song, G. A. Attard, T. Düren, F. Marken, *ChemElectroChem* **2019**, *6*, 252–259.
[11] A. Mahajan, S. K. Bhattacharya, S. Rochat, A. D. Burrows, P. J. Fletcher, Y. Y. Rong, A. B. Dalton, N. B. McKeown, F. Marken, *ChemElectroChem* **2019**, *6*, 4307–4317.
[12] F. Marken, E. Madrid, Y. Z. Zhao, M. Carta, N. B. McKeown, *ChemElectroChem* **2019**, *6*, 4332–4342.
[13] E. Madrid, N. B. McKeown, *Curr. Opin. Electrochem.* **2018**, *10*, 61–66.
[14] L. Wang, Y. Zhao, B. Fan, M. Carta, R. Malpass-Evans, N. B. McKeown, F. Marken, *Electrochem. Commun.* **2020**, *118*, 106798.
[15] A. R. Antonangelo, N. Hawkins, M. Carta, *Curr. Opin. Chem. Eng.* **2022**, *35*, 100766.
[16] P. M. Budd, B. S. Ghanem, S. Makhseed, N. B. McKeown, K. J. Msayib, C. E. Tattershall, *Chem. Commun.* **2004**, 230–231.
[17] E. Madrid, Y. Y. Rong, M. Carta, N. B. McKeown, R. Malpass-Evans, G. A. Attard, T. J. Clarke, S. H. Taylor, Y. T. Long, F. Marken, *Angew. Chem. Int. Ed.* **2014**, *53*, 10751–10754.
[18] Y. Y. Rong, Q. L. Song, K. Mathwig, E. Madrid, D. P. He, R. G. Niemann, P. J. Cameron, S. E. C. Dale, S. Bending, M. Carta, R. Malpass-Evans, N. B. McKeown, F. Marken, *Electrochem. Commun.* **2016**, *69*, 41–45.
[19] S. D. Ahn, A. Kolodziej, R. Malpass-Evans, M. Carta, N. B. McKeown, S. D. Bull, A. Buchard, F. Marken, *Electrocatalysis* **2016**, *7*, 70–78.
[20] Y. Z. Zhao, N. A. Al Abass, R. Malpass-Evans, M. Carta, N. B. McKeown, E. Madrid, P. J. Fletcher, F. Marken, *Electrochem. Commun.* **2019**, *103*, 1–6.
[21] J. S. Bonso, G. D. Kalaw, J. P. Ferraris, *J. Mater. Chem. A* **2014**, *2*, 418–424.
[22] Q. L. Yang, W. L. Li, C. Dong, Y. Y. Ma, Y. X. Yin, Q. B. Wu, Z. T. Xu, W. Ma, C. Fan, K. N. Sun, *J. Energy Chem.* **2020**, *42*, 83–90.
[23] C. Y. Li, A. L. Ward, S. E. Doris, T. A. Pascal, D. Prendergast, B. A. Helms, *Nano Lett.* **2015**, *15*, 5724–5729.
[24] M. Gigli, J. A. Kowalski, B. J. Neyhouse, A. D'Epifanio, F. R. Brushett, S. Licoccia, *Electrochem. Commun.* **2019**, *107*, 106530.
[25] L. Wang, Y. Zhao, B. Fan, M. Carta, R. Malpass-Evans, N. B. McKeown, F. Marken, *Electrochem. Commun.* **2020**, *118*, 106798.
[26] D. Ramimoghadam, S. E. Boyd, C. L. Brown, E. M. Gray, C. J. Webb, *ChemPhysChem* **2019**, *20*, 1613–1623.
[27] Z. X. Low, P. M. Budd, N. B. McKeown, D. A. Patterson, *Chem. Rev.* **2018**, *118*, 5871–5911.
[28] V. Vij, S. Sultan, A. M. Harzandi, A. Meena, J. N. Tiwari, W. G. Lee, T. Yoon, K. S. Kim, *ACS Catal.* **2017**, *7*, 7196–7225.
[29] W. Zhang, D. H. Li, L. Z. Zhang, X. L. She, D. J. Yang, *J. Energy Chem.* **2019**, *39*, 39–53.
[30] J. Aldana-Gonzáles, M. Romero-Romo, J. Robles-Peralta, P. Morales-Gil, E. Palacios-González, M. T. Ramírez-Silva, J. Mostany, M. Palomar-Pardavé, *Electrochim. Acta* **2018**, *276*, 417–423.
[31] M. Heuchel, D. Fritsch, P. M. Budd, N. B. McKeown, D. Hofmann, *J. Membr. Sci.* **2008**, *318*, 84–99.
[32] R. Chen, C. J. Yang, W. Z. Cai, H.-Y. Wang, J. W. Miao, L. P. Zhang, S. L. Chen, B. Liu, *ACS Energy Lett.* **2017**, *2(5)*, 1070–1075.
[33] D. P. He, Y. Y. Rong, M. Carta, R. Malpass-Evans, N. B. McKeown, F. Marken, *RSC Adv.* **2016**, *6(11)*, 9315–9319.
[34] P. M. Budd, E. S. Elabas, B. S. Ghanem, S. Makhseed, N. B. McKeown, K. J. Msayib, C. E. Tattershall, D. Wang, *Adv. Mater.* **2004**, *16*, 456–459.
[35] R. Chen, C. Yang, W. Cai, H.-Y. Wang, J. Miao, L. Zhang, S. Chen, B. Liu, *ACS Energy Lett.* **2017**, *2*, 1070–1075.
[36] A. J. Bard, L. F. Faulkner, *Electrochemical Methods*, 2nd ed., Wiley, New York, **2001**.
[37] S. Park, Y. C. Hu, J. O. Hwang, E. S. Lee, L. B. Casabianca, W. W. Cai, J. R. Potts, H. W. Ha, S. S. Chen, J. Oh, S. O. Kim, Y. H. Kim, Y. Ishii, R. S. Ruoff, *Nat. Commun.* **2012**, *3*. 638.
[38] C. K. Chua, M. Pumera, *Chem. Commun.* **2016**, *52*, 72–75.
[39] F. Kim, J. Y. Luo, R. Cruz-Silva, L. J. Cote, K. Sohn, J. X. Huang, *Adv. Funct. Mater.* **2010**, *20*, 2867–2873.

Manuscript received: December 22, 2023
Revised manuscript received: March 22, 2024
Version of record online: ■■, ■■

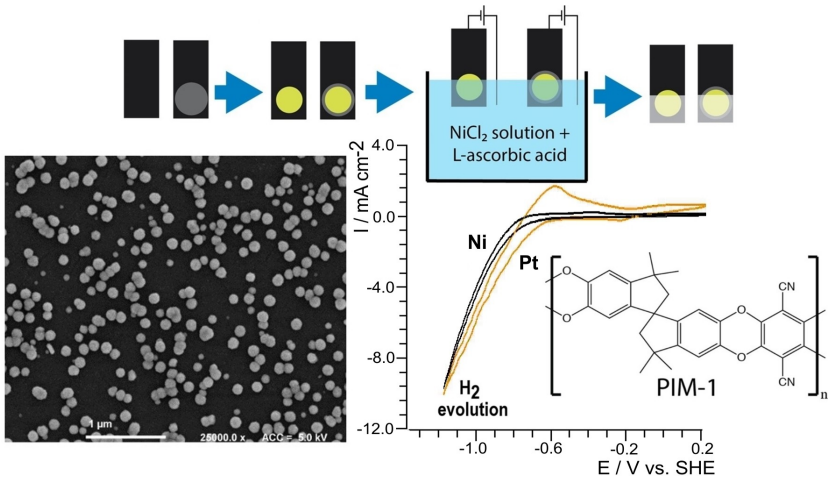

Nickel electrodeposition into a thin layer of polymer of intrinsic microporosity (PIM-1) coating yields well-defined metal nanoparticles, resulting in an enhanced catalytic hydrogen evolution by suppressing the gas-bubble blocking effects. With respect to platinum based-nanoparticles, on the same substrate, such an electrocatalyst has a comparable onset value for hydrogen evolution.

J. Isopi, N. B. McKeown, M. Carta, G. Tuci, G. Giambastiani, M. Marcaccio, F. Marken**

1 – 10

Thin Coatings of Polymer of Intrinsic Microporosity (PIM-1) Enhance Nickel Electrodeposition and Nickel-Catalyzed Hydrogen Evolution